SPACECRAFT

PARTICULATE SIZING SPECTROMETER

by

Henry A. Miranda, Jr.

7 April, 1992

FINAL REPORT
SUBMITTED TO NASA GODDARD SPACE FLIGHT CENTER
UNDER
CONTRACT NAS5-30306

MIRANDA LABORATORIES
74 Loomis Street
Bedford, MA 01730

1.0 INTRODUCTION

A new type of single-particle sizing spectrometer has been developed by Miranda Laboratories under NASA/GSFC SBIR sponsorship for application to spaceborne monitoring and particle research needs. This report describes the main features of a working prototype device recently delivered to the sponsoring agency for evaluation. Although the description is limited in scope owing to the proprietary nature of certain key design elements, it provides sufficient information to gain an understanding of its operation, and permits the reader to gain insight concerning the potential utility of such a device as a workhorse sensor for the purposes mentioned above. Recommendations for a flight demonstration unit are also included.

The well-known principle of forward scattering is exploited to detect and to measure the diameter of individual particles that cross a carefully controlled remote sensing zone. As in all such devices, the resulting light collected within a predetermined range of off-axis scattering angles is linked to the diameter of the particle by means of Mie theory, (REF 1, 2). However, unless special precautions are taken to ensure that this linkage is carefully preserved in the design, (REF 3), serious degradation in sizing accuracy will occur.

All of the relevant factors which could adversely affect the above linkage have been taken into account and eliminated in this prototype. Chief among these are design details concerning means for : 1) controlling the location, the shape, and the illumination profile within the sensing zone, 2) minimizing all unwanted light that is scattered by elements within both the transmitter and the receiver modules, and 3) achieving low noise operation in the detection circuitry.

The resulting success in meeting the original design goals set for this particular configuration provides confidence in being able to assert that spaceborne particulate sizing can indeed be performed with such a device. Beyond this, it is also shown below that the basic embodiment lends itself readily to modifications, (e.g., by trading off one design ingredient for another), to meet any of several different objectives that might emerge as dominant needs for future space operations.

2.0 PROTOTYPE CONFIGURATION

This particular embodiment was designed to demonstrate that follow-on flight hardware can be housed in two adjacent GAS canisters, without sacrificing the main objective of sizing individual particles in the 5-50 micron diameter range. Figure 1 shows a schematic view of the system, with the transmitter in one canister and receiver in the next, (both of which use Motorized Door Assemblies).

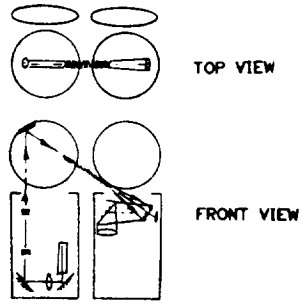

FIGURE 1: Two-canister configuration

A near-infrared pulsed laser diode transmitter, together with beam-shaping optics and beam-steering mirror, is housed in the canister on the left, while both the receiving optics and signal processing electronics, together with ancillary control circuitry, etc., is housed in the other. (In the prototype unit, a separate desk-top PC/AT is used to perform all calculations, whereas in the flight hardware, this function will be performed by a hardened data acquisition/recording module.)

The remote sensing zone, (which in this instance is a ribbon-shaped beam 10mm wide, one mm thick and about 300mm in length), is located above and between the canisters. It is tilted at an angle of about 30 degrees, as shown. The receiving system collects the light scattered in three small forward scattering annuli, the largest of which is 2.60 degrees.

The beam-steering mirror is mounted to a fixed member which extends about 20 inches above the transmitter canister. This particular feature, (which was added as a no-cost extension, and is therefore in a breadboard configuration), demonstrates its basic feasibility. In the flight hardware, this was to have been mounted on a deployable fixture protruding through the top of the experiment mounting plate.

The two-canister arrangement was based on the assumption that the placement of a separate mirror external to the canister would render the operational interface awkward (in the context of the GAS philosophy). It has since been learned, however, that such a constraint no longer applies. Thus it is possible to configure the system so that it fits into a <u>single</u> canister, (with an auxiliary mirror which is totally passive, and fixed at a specific external location). Such a configuration, which has certain very notable advantages over the present one, is discussed in greater detail in Section 6 below.

3.0 THE USE OF FORWARD SCATTERING

When a particle is illuminated, light is scattered in all directions. The amount of scattered light collected by a given receiving channel , (F_s) is given by:

$$F_s = \left[\frac{\lambda}{2\pi} \right]^2 (I_{av})(\Omega)(T)_o(F_o) \quad \ldots\ldots\ldots\ldots\ldots\ldots (1),$$

where: (F_o) is the beam illumination level (Watts/cm^2),

(Ω) is the solid angle subtended by the receiving optics at the scattering point,

(T) is the detector channel throughput,

(λ) is the illumination wavelength, (cm), and

(I_{av}) is the (dimensionless) Scattering Parameter. This latter parameter, which is calculated using Mie theory, is a function of: 1) the scattering angle, 2) the particle refractive index, and 3), the particle diameter. The Scattering Ratios, (F_s/F_o) observed by three separate detector channels at their respective angles, are used to determine the particle diameter.

It is presumed in the above that the particle is spherical. While few particles fit this assumption perfectly, it is generally felt that departures from this condition are of less concern in spaceborne environments than under most earth bound circumstances. At any rate, an assessment of the sizing error resulting from this assumption in devices that use forward scattering has been conducted under this program. A discussion of this phenomenon, together with specific results that provide a quantitative insight into the error, (for spheroids as a function of the asymmetry parameter), is presented in Appendix I.

For particles with circumference larger than the wavelength, (which is the case here), it is sometimes useful as a general rule to think of the forward-lobe scattering parameter as being proportional to the projected area of the particle, (for single wavelength, index of refraction, and scattering angle). This form of characterization is extremely limited, however, for upon this general proportionality are superimposed certain very significant undulations with increasing particle size. These undulations can be envisioned as comprising two separate components:

1- large-scale undulations of very large amplitude, and
2- small-scale undulations of much smaller amplitude.

A typical example of such behaviour is seen in Figure 2: the larger-scale undulations are the dominant source of sizing ambiguities, (which can best be termed as ubiquitous), while the smaller undulations aggravate the situation.

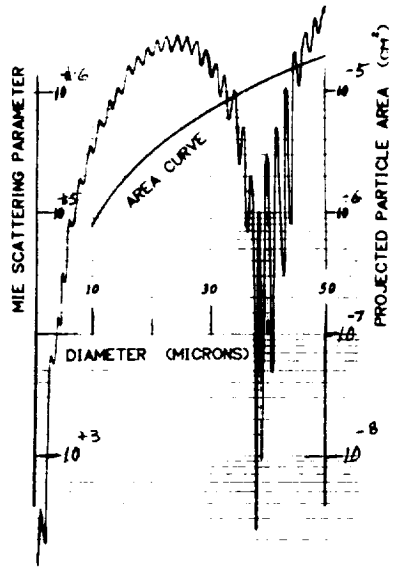

FIGURE 2: Mie Scattering Undulations

A key feature of the present device lies in the fact that a means has been found to reduce the number of such ambiguities to a relatively insignificant, (and thus very manageable) few. Moreover, based upon our results to date, it is felt that these ambiguities can be eliminated with relatively straightforward modifications.

Additional features of the device are that the particle size output is: 1) totally independent of particle index of refraction, and 2) largely insensitive to particle shape as well. This is of special significance in view of the likelihood that spaceborne particulates many be 1) composite and 2) non-spheres.

4.0 SPECIFIC SYSTEM PARAMETERS

4.1 Transmitter Module

This module is comprised of the laser diode source, driving electronics, pulse synchronizing circuitry, beam-shaping optics, and a two-axis beam-steering mirror, (the latter having been

provided as a breadboard item as noted previously). The source, which dissipates about 15 watts, has been designed to permit long term stable operation without any need for active cooling measures. The output, (whose wavelength is at 0.905 micron), consists of a continuous set of 200-nanosecond pulses at 3.4 kilohertz. The peak power at the center of the flat ribbon sensing zone during each pulse is about 13 Watts/sq.cm. A lateral profile of the beam is shown in Figure 3.

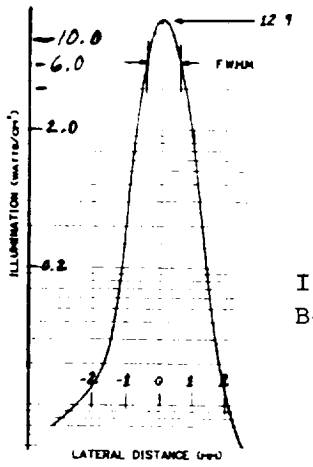

FIGURE 3:

Illumination Beam Profile

The synchronizing circuitry, (which detects a tiny fraction of unused light within the transmitter optics cavity), generates an appropriate signal at the occurrence of each pulse, and alerts the signal processing electronics to sample the detector outputs in sequence. Since this sensor was situated in the Transmitter for convenience in the prototype, a separate cable was required between the transmitter and receiver modules. This cable can be eliminated in the flight unit, because it is not essential that the synchronous detector be located in the transmitter.

The beam-steering mirror is driven by a galvanometer whose input is derived from a quadrant detector (located in a beam dump compartment within the receiver module). The signal processing software computes the required feedback voltages to keep the beam in the desired direction. These are updated at a maximum rate of about 1/8 sec. (The operating parameters of this feedback network are not optimized, owing to its breadboard nature.) An auxiliary software routine permits the operator to place the beam close to the center of the receiver opening, (the objective being to ensure solely that the quadrant detector is illuminated by the beam), by means of keyboard inputs to the computer. Once this condition is achieved, the beam is brought to its proper center position by the control logic.

It is important to note that the flight unit will require a fully automatic system. This must include acquisition capability, wherein a coarse control system with very broad angular field acts initially to place the beam within the operating range of the fine control system. In a sense, one can envision this as substituting for the role of the human operator in the prototype hardware.

4.2 Receiver Module

This module contains the receiving optics, 3-channel detector system, and Beam Dump, (which includes the quadrant detector as noted in the previous section). A hole in the center of the first mirror element permits the unscattered light to pass through and be directed to the Beam Dump. The quadrant detector serves two ends: 1) The individual element outputs are used by the beam steering logic, and 2) the sum output is used in generating the scattering ratios, which determine the particle size.

The three signal detector channels achieved the requisite noise levels of (0.3-1.0) nanowatts by using charge amplifiers as well as battery bias, (45 volts), the latter utilizing very short leads so as to preserve high rise times. Because of the extremely low current drain on these batteries, they are expected to last for perhaps several years, (which justified the use of the dry-cell variety in this instance). Thus, provision for ready replacement of these in the prototype device was not necessary.

In the case of the flight unit, however, the possibility of incurring lengthy delays precludes the use of dry-cells for this purpose. Therefore provision must be made either for an ultra-low-noise power supply, or rechargeable batteries. In the latter instance, care must be taken to ensure that the recharging leads are properly isolated so as to avoid picking up unwanted coherent noise originating from the transmitter circuitry.

4.3 Internal Stability

The transmitter and receiver modules were both subjected to the NASA GAS canister shake environment (as specified in the Experimenter Handbook, 1987), at NTS, a nearby environmental test facility. Upon return to Miranda Laboratories, the transmitter beam location, beam intensity, synchronous detector parameters, receiver detector sensitivities and noise levels, receiver optics, and quadrant detector parameters, were tested, and found to be unchanged from their pre-shake values.

Subsequent operation revealed a susceptibility to a steady lateral bending moment on the transmitter module. This is unique to the prototype, since such forces would not be experienced in the flight unit. At any rate, the nature of the susceptibility was examined, and is clearly understood: It originates from the presence of a narrow slit field stop in the transmitter module optics, through which a line-like image of the light must pass. The lateral tolerance of this combination is measured in tens of microns along the short dimension. Bending of the optical train in this direction was sufficient to shift the lateral location of the image in relation to the slit, thereby reducing the light passing through by a significant amount. Because this design deficiency can easily be rectified, there is no reason to avoid incorporating the requisite modifications into the flight unit.

4.4 Data Processing System

As each particle crosses the sensing zone, it experiences steadily increasing beam illumination until it reaches the center, beyond which the illumination diminishes. The scattered light collected by all three detecting channels follows this pattern. Since the illumination is pulsed at 3.4 kilohertz, it follows that a half-micron particle crossing perpendicular to the flat ribbon at a speed of 1.4 ft/sec, (= 425 mm/sec) would develop 4 pulses above the noise level before arriving at the beam center, (the fifth pulse occurring just after having passed this point). (A larger particle of the same speed would develop more pulses before having arrived at the center of the beam, owing to the fact that the beam profile does not have infinitely steep walls, but exhibits wings, as may be seen from Figure 3 above.)

The data processing system demands that a minimum of four sequential pulses above a given user-selected threshold level be observed, each being higher than the preceding one, in order for it to recognize that a particle has been detected. Once this condition is fulfilled, it then searches for the first indication of a pulse smaller than the preceding one, upon which further tracking ceases. The pulse heights for that prior pulse in all three channels are recorded, as well as the sum of the four quadrant detector outputs.

The observed Scattering Ratios in Eq. (1) are calculated, and the particle size is then determined, (after subtracting the measured background levels from each of the detector channel outputs, as will be discussed presently), using a table look-up routine which incorporates the system constants of Eq. (1) and the Scattering Parameter data, together with the calibration constants of the system, (the latter being determined by separate means). The Particle Count stored in the appropriate size bin register is incremented by one, and the system is ready to observe the next particle.

Since a minimum of five adjacent pulses are involved in the detection of each particle, (see below), the sizing ability begins to degrade if the temporal spacing of the particles is less than (5/3400) = 1.47 millisec. For particles crossing perpendicular to the ribbon plane at the above speed, this is equivalent to a maximum particle rate of about 700/sec. (As the angle of their trajectory becomes more parallel to the plane of the flat ribbon, this rate will of course decrease.)

The above limitation can be expressed in a more general sense by relating it to a spatial frame, rather than a temporal frame. Degradation cannot begin to occur until particle separations shrink to less than about one foot, (which translates to a concentration of about one/cubic foot, or 35/cubic meter). This restriction would apply to uncontrolled flow fields, such as might pertain under spaceborne conditions. In the laboratory, however, (where the particles can readily be produced in the form of a sheet, for example), the linear spacing can be very much higher, (i.e., about one per cubic centimeter).

The use of a threshold level as noted above circumvents the possibility of noise, (or of large concentrations of very small particles), usurping a disproportionate amount of processing time. (It should be noted in this connection that any particles entering the sensing zone while the system is churning with non-particles in this manner, are simply not observed.) This capability is very useful under laboratory conditions because of the relatively large particle concentrations that are usually involved. However, it is not clear that the concentrations of spaceborne flow fields will be high enough to warrant the retention of such a flexibility in the flight unit. While such a feature would not overly complicate the flight hardware, it would impose an additional decision on the user which may not be justified if the unit is to be flown only once. (On the other hand, if it is expected to be flown on several flights, this feature might be quite advantageous, since it would allow adjustments between flights to this parameter in accordance with updated —— or changing —— flowfield parameters.)

4.5 System Outputs

A very simple user-friendly, menu-driven software package is provided which permits the user to select one of several counting alternatives: 1) a specific start and stop time, 2) a specified time interval ensuing from a start command, 3) a specific number of particle counts to be detected, and 4) an unspecified period of continuous data collection until a stop command is issued.

The system, upon receiving a start command, calculates the average detector output value from the first 100 illumination pulses (together with the RMS deviation therefrom), for each of three detection channels, as well as each of the four quadrant detector channels. These data, which are displayed on the monitor screen in tabular form on command, are developed without regard to the possibility that a particle might be present in the sample and thus contaminate the background determination.

It is pointed out that the chance occurrence of a particle during the background measurement interval is readily noticeable after the fact, since this is manifested as an excessively large RMS value in relation to the to Mean value. When the unit is operated in a clean room, this problem is totally avoided. When operated under normal room air conditions, (without any conscious effort to stir up room dust), the probability of such background contamination is small, (though not zero). Whenever this occurred
in practice, the run was simply repeated. During flight, however, it may turn out to be inconvenient to collect this background data when the particulate concentrations are known to be very low.

The adverse thermal environment of spaceflight must also be taken into account. The fact that excellent background stability has been observed with the prototype unit could be turned to good advantage in this regard: The functional relationship between the temperature and associated changes in detector background levels can be established by experiment in advance; and a suitable means can be devised for: a) sensing the actual temperature experienced in real time during the flight, and b) applying the necessary correction factors to the measured pre-flight, fixed-temperature background levels in the software.

An alternate approach would modify the present software routine in the sequence of actions at the commencement of a given data run to: a) inspect the observed (RMS/Mean) ratios and b) repeat the entire background measurement whenever any of these ratios exceeds a predetermined value. This alternative appears to be intuitively more satisfactory, in that it involves less complex hardware, and also closes the loop at a more opportune point.

As each particle is detected, the resulting peak values, which represent the sum of signal plus background in each of the three detector channels, (see Section 4.4 above), are reduced by these background values to derive the associated signal levels. At the end of a given run, a histogram depicting the total number of particles counted in each of ten adjacent sizing bins between 5 and 50 microns, is generated. Three additional items of sizing data are also provided: 1) the number of particles smaller than five microns, 2) the number of particles larger than 50 microns, and 3) the number of particles which are unintelligible in terms

of size. The first two are assigned to respective bins at opposite ends of the histogram, whereas the third item is simply displayed as a specific number of "missed particles", which is written above the histogram.

The term "missed" particles signifies the number of particles for which the ratios of peak signals in the three detection channels does not fit the calculated ratios for any of the size bins. Each of these misfits is evidence that either: a) the particle departs very seriously from a sphere, or b) the peak "signal" is not that of a single particle, but the conglomerate result of two or more particles in the beam during the sampling period. This latter situation would prevail whenever a second particle enters the beam while the search for a peak value is in progress, (i.e., before the first particle has experienced the peak illumination). Thus the number of "missed" particles, when compared to the total number processed in a given histogram, is an objective measure of of the internal consistency of the data.

4.6 Sizing Ambiguities and Resolution

The existence of certain specific sizing ambiguities in this prototype unit has arisen from the fact that several optical parameters had already been established prior to having discovered these idiosyncrasies in the calculation scheme used to develop the particle sizes from the measured pulse heights. Since the origins of these ambiguities are well understood, they can be minimized in the flight unit by careful matching of the optical parameters to the specific results of the Mie calculations.

A related factor which affects sizing resolution should also be pointed out. The sizing bins are uniform, (i.e., 2.5 microns), whereas the sizing uncertainties derived from the pulse height data, (termed "bands" here), are not uniform, (the latter being in some instances larger, while in others, smaller than the former). The binning algorithm used in the prototype unit simply assigns a particle to a given bin if the upper extreme of the calculated sizing band falls within that bin, (without regard to the location of the lower end of that same sizing band). An appropriate modification to the algorithm will be incorporated in the flight unit design. This will likely follow the approach of distributing the "count" in accordance with the band size.

5.0 SYSTEM OPERATION AND RESULTS OBTAINED

Calibration of the system was achieved by injecting particle streams of both 10- and 15-micron diameter monodisperse spheres of Polystyrene-latex across the sensing zone, and adjusting the appropriate software constants to yield the proper location of the peak size distributions in both of the respective histograms. Since the associated detector pulse heights are about an order of magnitude apart from one another, these two sizes are well matched to the system parameters for this purpose.

Following this, a series of runs using different powdered materials, (Aluminum Oxide, Silicon Carbide, and Talc), were performed. In each instance the powder had previously been passed through calibrated sieves for the purpose of establishing a size

"cut" point for that particular batch. Since all of these are crystalline materials, they exhibited significant departures from true spheres. In spite of this, however, results obtained in all cases indicated reasonably good agreement with what had been anticipated on the basis of the sieve cut point. This agreement was further corroborated by visual comparison data of the same samples collected with a microscope.

An additional factor lending credence to the validity of the system concept with regard to its relative insensitivity to particle shape, lies in the fact that the proportion of "missed" particles in the histograms was in all cases very small. It is recalled from Figure 2 above that rather large nonlinearities are inherent in the functional relationship between angular scattering profile and particle size. Thus, the scattering ratios for all three channels are tightly coupled to one another. If significant departures from the calculated ratios, (which apply to spheres), were to prevail in these detected signals, then the measured ratios would simply not fit, and a large number of particles would be classified as "missed". Since this did not occur, it follows that the system yields good sizing information for non-spherical particulates.

The use of crystalline material for these tests served as a good approximation to the non-sphericity that is expected to prevail in spaceborne particulates. Hence the above results are viewed as extremely encouraging.

6.0 CONCLUSIONS AND RECOMMENDATIONS

Based upon the achievements of the prototype unit described in the preceding sections of this report, it is concluded that the main objectives of the Phase-II development effort have been met. More specifically, it has been further demonstrated that:

- remote sizing of individual particles in the 5-50 micron range for ultimate use in spaceborne applications, can be performed,
- a demonstration flight unit can be housed in two adjacent GAS canisters,
- sizing is independent of particle refractive index,
- sizing is reasonably accurate, even for crystalline matter that departs significantly from spheres, and
- sizing is independent of location within the sensing zone.

All of the major technical concerns that might have placed such a capability in the category of "high-risk" technology, have been addressed during this program and resolved favorably. In addition it has been learned that earlier constraints thought to preclude fitting the system into a single GAS canister, have been found no longer to apply. It is therefore concluded that such a device is eminently feasible.

The outlines of a follow-on flight unit that have emerged as an outcome of the foregoing development effort can be readily established, and are set forth below. Such a device would serve two separate purposes simultaneously:

1- It would demonstrate that such a capability is a practical reality within present-day technology.
2- It would commence the process of developing a much-needed data base for characterizing particulate environments on spaceborne platforms.

The description of the prototype system in the preceding sections incorporated several specific references to design elements that require modifications in progressing to an actual flight system. Because these items were treated in the context of the respective topics under consideration, they are distributed throughout the report, and are therefore difficult for the reader to formulate into a cohesive set of requirements applicable to the recommended follow-on flight hardware. It is therefore useful to collect the topics as a single set of specific areas that need to be addressed in the final design of such a flight unit:

1- the incorporation of a dedicated, flight-worthy computer and output histogram-storage module,
2- a means for permitting the user to set a predetermined sequence of measurements along the flight timeline,
3- the development of a fully automatic beam acquisition and control system,
4- a means for ensuring that background level measurements of the separate detector channels are not contaminated with chance particulates,
5- the elimination of residual sizing ambiguities and sizing resolution degradation.
6- a reconfiguration of the system to fit entirely within a single canister.

All of the above items have been carefully considered, and none have been found to involve problems that would seriously impede the straightforward development of a suitable flight unit.

With respect to item #6 above, the system would require positioning an external mirror at a suitable fixed location situated above the canister opening. The precise distance of the mirror, (and also the elevation angle of the beam with respect to the canister top), will be determined upon discussion with the appropriate NASA personnel who are responsible for assigning the requisite mirror mounting area. This must be fixed before the final receiver parameters can be determined.

With respect to item #2, the necessity for a completely self-contained operation sets limits on the total energy available during a given flight. This in turn imposes a need for periods of quiescence. These latter would be suitably matched to foreknown timeline events, which would likely differ from flight to flight.

5.1 Other Trade-off Possibilities

The practical viability of the underlying principle has been established in terms of one specific embodiment for detecting spaceborne particulates. This focused only on a single particular spaceborne environment monitoring need. There are, however, a variety of other particulate environment parameters which can be met with different embodiments resting on the same principle of operation.

For example, the sizing capability of the present prototype was attained by exercising very precise control of the scattering angles. In order to achieve this objective, a rather severe set of design constraints had to be imposed on both the transmitter and receiver modules. This in turn has resulted in a relatively small sensing zone.

It follows that, if one were willing to relax the sizing capability, a much larger sensing zone could be achieved, (and in addition, the need for multiple detection channels would be eliminated, thereby reducing the overall system complexity). This would at the same time permit extending the size threshold down to the (0.5 - 1.0 micron) regime. Under this latter circumstance, it clearly is possible to trade off sensing zone area coverage for size threshold limits.

The availability of excess signal opens up yet another possibility, namely to determine individual particle speed and/or direction. In this latter connection, several alternatives are envisioned. These span across a spectrum of possibilities, at one end of which are embodiments which would yield crude directional information of the individual particles.

At the other end of the spectrum is a full-fledged capability for the characterization of particulate flow-fields in real time. Such a device, (REF 4), would not only sense the speed, direction, and location of individual particles crossing a rather large sensing zone, but also would determine the location of the source as well. In addition, it would permit a determination of the lateral extent of the source, (assuming that the angle of divergence were sufficiently large).

7.0 REFERENCES

REF 1- "Light Scattering by Small Particles", H. C. van de Hulst, Wiley, N.Y., 1957.

REF 2- "The Scattering of Light and Other Electromagnetic Radiation", M. Kerker, Academic Press, N.Y., 1969.

REF 3- "Atmospheric Aerosols, Their Formation, Optical Properties and Effects", (A. Deepak, Ed.) pp 361-380, (article entitled, "Instrumentation Design Factors Affecting the Accuracy of Particulate Size Distribution Measurements", by H. A. Miranda, Jr.), Spectrum Press, Hampton, VA., 1982.

APPENDIX I

DEPENDENCE OF SCATTERING AMPLITUDE ON ECCENTRICITY OF SPHEROIDS

RICK MIRANDA AND HENRY A. MIRANDA, JR.

1. Introduction

This appendix investigates the sensitivity with respect to eccentricity of electromagnetic scattering in the forward direction by dielectric spheroids. Spheroids represent a relatively simple, yet adequate approximation to non-spherical particulates generally believed to comprise the spaceborne environment. Though necessarily limited in scope, the investigation is nonetheless quite useful in that it provides a sound theoretical basis supporting the assertions in the main body of the report (as well as the rudimentary experimental findings), namely that the particulate sizing output of the instrument is largely independent of particle shape. The fundamental problem of this investigation is to find a good approximation to the scattering amplitudes; formulas due to Holt and Shepherd [1] are used here. These formulas are for forward scattering only, at angle $\theta = 0$, and are described briefly in the next section.

2. The Approximate Scattering Amplitude Formula

In [1], Holt and Shepherd develop an approximate forward scattering amplitude formula for Van de Hulst scattering of spheroids. Let the spheroid have major axis a and minor axis c, and be composed of material of (complex) index of refraction m. Assume that incoming light of wavelength λ is pitched at angle θ' with respect to the semimajor axis of the spheroid. Let

$$c_{33} = \frac{\sin^2(\theta')}{a^2} + \frac{\cos^2(\theta')}{c^2},$$

$$k = 2\pi/\lambda,$$

and

$$\mu = \frac{2k(m-1)}{\sqrt{c_{33}}}.$$

Holt and Shepherd's formula for the approximate forward scattering amplitude is then

$$f_{a,c}(\lambda, m, \theta', 0) = (ika^2c\sqrt{c_{33}}/\mu^2)[1 + \mu^2/2 - e^{i\mu}(1 - i\mu)]. \tag{2.1}$$

This is formula (27) in [1]; the 0 in the formula definition as the last parameter refers to the forward scattering. The formula is obtained using a cross-section argument following a derivation in Newton [2]. It agrees well when $a = c$ (the sphere case) with the corresponding formulas in Van de Hulst's book [3] for indices not far from 1, (which latter have been utilized as the basis for the design of the instrument, as discussed in the body of the report above). The wavelength λ in this project was set to 0.9 microns for every computation.

March 31, 1992.

For simplicity, the incoming angle θ' was set to 0 for every computation. This simplifies the above quantities to

$$c_{33} = 1/c^2, \mu = 2k(m-1)c,$$

and the formula (2.1) becomes

$$f_{a,c}(\lambda, m, 0, 0) = (ika^2/\mu^2)[1 + \mu^2/2 - e^{i\mu}(1 - i\mu)]. \tag{2.2}$$

It should be noted that the quantities observed by the instrument are the scattered intensities, which are the squares of the amplitudes.

3. The Dimensions of Equivolumetric Spheroids

Let $S(r)$ be a sphere of radius r. In this section we will derive the formulae for the major and minor axes a and c of the spheroid $F(a, c)$ with the same volume as $S(r)$, with a given eccentricity e.

Recall that $F(a, c)$ is the ellipsoid with three radii a, a, and c. The volume of an ellipsoid $E(a, b, c)$ with radii a, b, and c is given by the formula

$$\text{vol}(E(a, b, c)) = \frac{4}{3}\pi abc.$$

Therefore the volume of the spheroid $F(a, c) = E(a, a, c)$ is

$$\text{vol}(F(a, c)) = \frac{4}{3}\pi a^2 c,$$

and the volume of the sphere $S(r)$ with radius r is

$$\text{vol}(S(r)) = \frac{4}{3}\pi r^3.$$

The eccentricity e of the spheroid $F(a, c)$ is defined to be the ratio

$$e = a/c.$$

Suppose now we are given the volume V and the eccentricity e of a spheroid F. We wish to determine the major axis a and the minor axis c such that $F = F(a, c)$. We must therefore solve the simultaneous equations

$$a = ec \text{ and } V = \frac{4}{3}\pi a^2 c$$

for the desired radii a and c. This leads to the solution

$$c = (\frac{3}{4}V/(\pi e^2))^{1/3} \text{ and } a = (\frac{3}{4}Ve/\pi)^{1/3}.$$

Now suppose further that $V = \text{vol}(S(r)) = \frac{4}{3}\pi r^3$ is in fact the volume of a sphere of radius r. Then the formulas above yield

$$a = a(r, e) = re^{1/3} \text{ and } c = c(r, e) = re^{-2/3}. \tag{3.1}$$

These are the major and minor axes of the equivolumetric spheroid.

4. The Programs Written for the Project

Two programs were written to support the effort of this appendix. The first and basic one was a subroutine to calculate the scattering amplitude formula (2.1); this was done, and the function was named "scatamp". The second program, entitled "eccen", used the subroutine "scatamp" to compute the ratio between the amplitudes for a perfect sphere and the equivolumetric spheroid of a given eccentricity.

Since the instrument outputs are proportional to the scattering intensities, which are the squares of the scattering amplitudes, we actually computed the ratio of the squares of the amplitudes. Specifically, for a range of radii r and eccentricities e, the ratio

$$R(r,e,m) = f^2_{a(r,e),c(r,e)}(0.9,m,0,0)/f^2_{r,r}(0.9,m,0,0)$$

was computed, using Holt and Shepherd's approximation (2.2). The quantities $a(r,e)$ and $c(r,e)$ were computed using the formulas (3.1). The wavelength $\lambda = 0.9$ microns and incoming angle $\theta' = 0$ were used uniformly in the project. A range of refractive indices were used, corresponding to interesting particles; specifically, runs were made with $m = 1.33$, $m = 1.7$, $m = 1.3 - 10^{-6}i$, $m = 1.55 - 8 \times 10^{-5}i$, $m = 1.75 - 10^{-6}i$, and $m = 1.55 - 6.58 \times 10^{-3}i$. Eccentricities ranged from $e = 0.7$ (oblate spheroids) to $e = 1.5$ (prolate spheroids); radii ranged from $r = 2.5$ to $r = 25$ microns.

The program "eccen" also computed average values $\hat{R}(e,m)$ for the ratio $R(r,e,m)$ for fixed e and m, averaged over the radius r.

These two programs were written in the C language. Implementations were developed on a PC (IBM-compatible) and on a Sun SPARCstation IPC workstation. This code is presented in Appendix 8.

5. Numerical Results

Figures 1, 2, and 3 contain typical plots of the ratio of scattering intensities R for the range of radii and eccentricities mentioned in the previous section, for the index $m = 1.33$.

Two features are notable in these figures. Firstly, for fixed eccentricity e, the plot of ratio R versus radius r is oscillatory, with a large wavelength (approximately 12 microns) superimposed on a smaller wavelength (approximately 1.5 microns). Moreover, there is evidence of damping in the larger radii. Finally, the oscillations vary over a constant mean value: there is no "trend" in the function. The second feature is that as the eccentricity increases, the ratio also increase.

Figure 4 shows a single plot (for $e = 0.8$ and $m = 1.33$) where the features for fixed eccentricity may be examined more closely. (Here the ratio of scattering amplitudes

$$f_{a(r,e),c(r,e)}(0.9,1.33,0,0)/f_{r,r}(0.9,1.33,0,0)$$

is shown, which is the square root of the ratio of scattering intensities R mentioned above.) The data on this plot are smoothed by averaging at each point the 5 on either side. One can see clearly here the two periodic phenomena, and the constant mean value (of about 0.862).

Figure 5 is a plot of the average ratio of amplitudes $\sqrt{(\hat{R})}$ as a function of the eccentricity, for various refractive indices. The striking feature of this graph is that, for all of the indices whose imaginary part is less than 10^{-4} in absolute value, the graph is the same. In other words, for small imaginary part, this average ratio is *independent of refractive index.* (It should be pointed out in this connection that the range of refractive index covered here applies to most materials likely to be encountered in the spaceborne environment.)

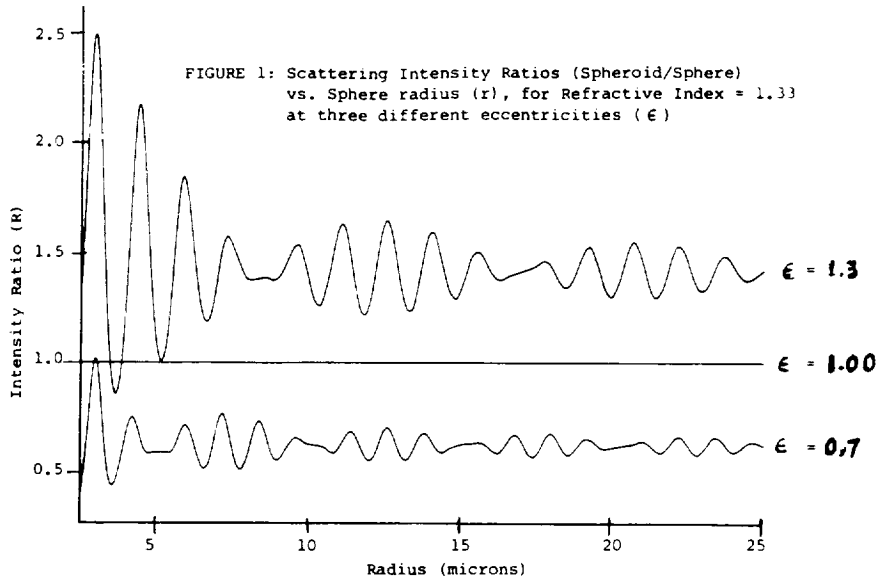

FIGURE 1: Scattering Intensity Ratios (Spheroid/Sphere) vs. Sphere radius (r), for Refractive Index = 1.33 at three different eccentricities (ϵ)

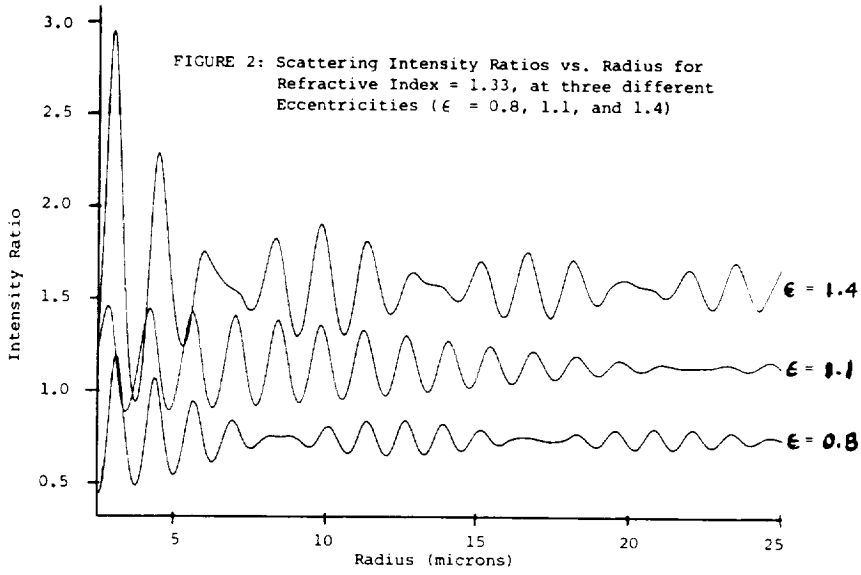

FIGURE 2: Scattering Intensity Ratios vs. Radius for Refractive Index = 1.33, at three different Eccentricities (ϵ = 0.8, 1.1, and 1.4)

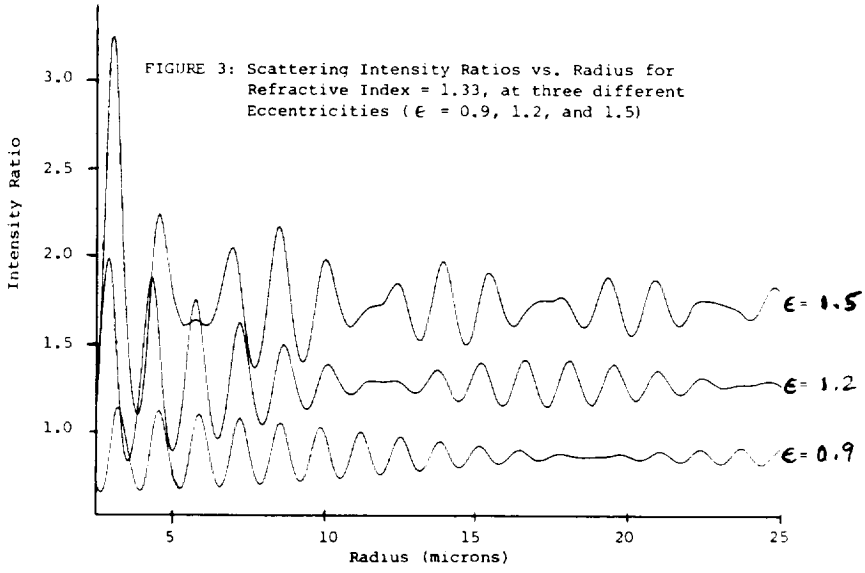

FIGURE 3: Scattering Intensity Ratios vs. Radius for Refractive Index = 1.33, at three different Eccentricities (ϵ = 0.9, 1.2, and 1.5)

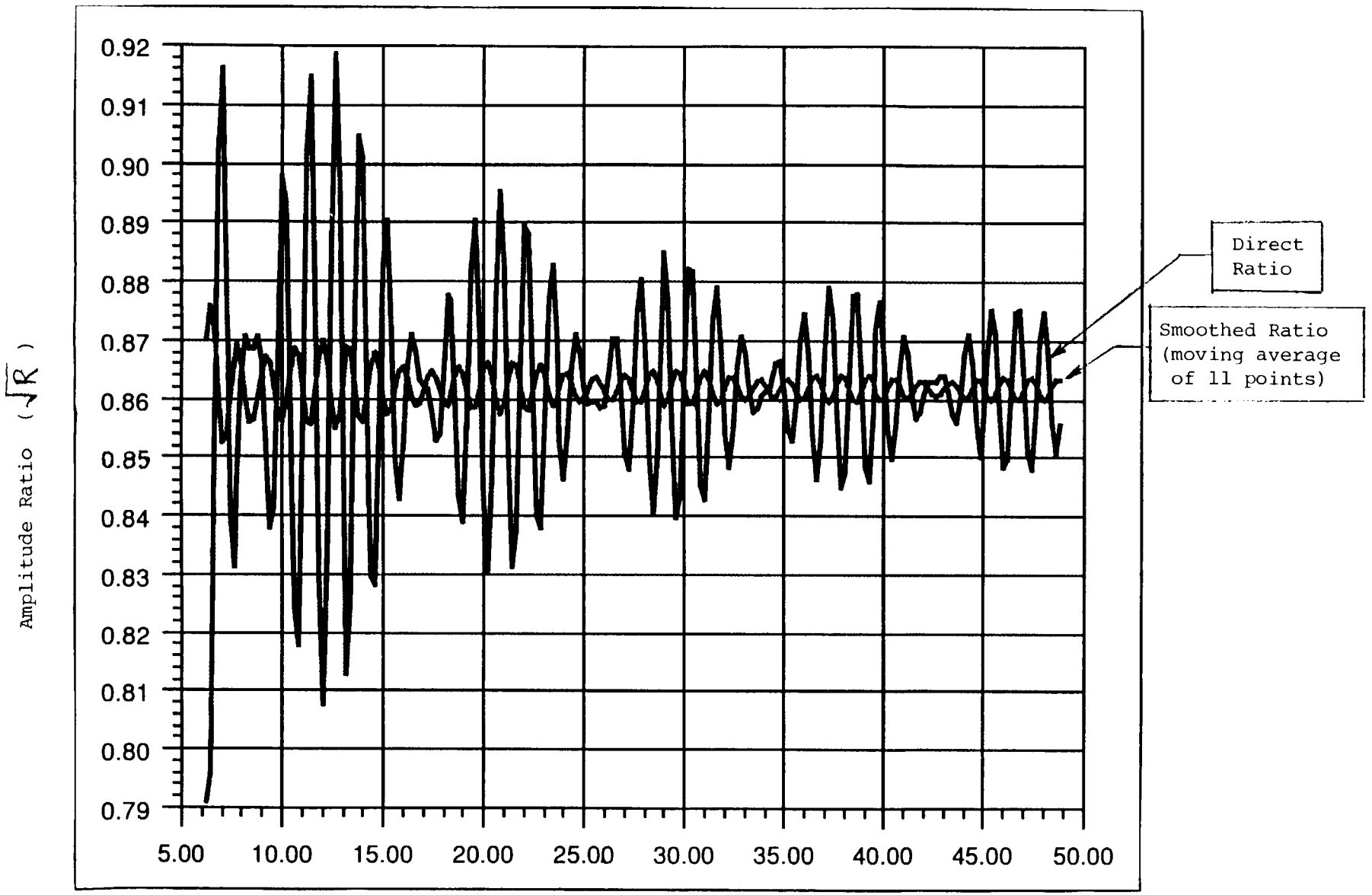

FIGURE 4: Amplitude Ratio versus Radius (microns)

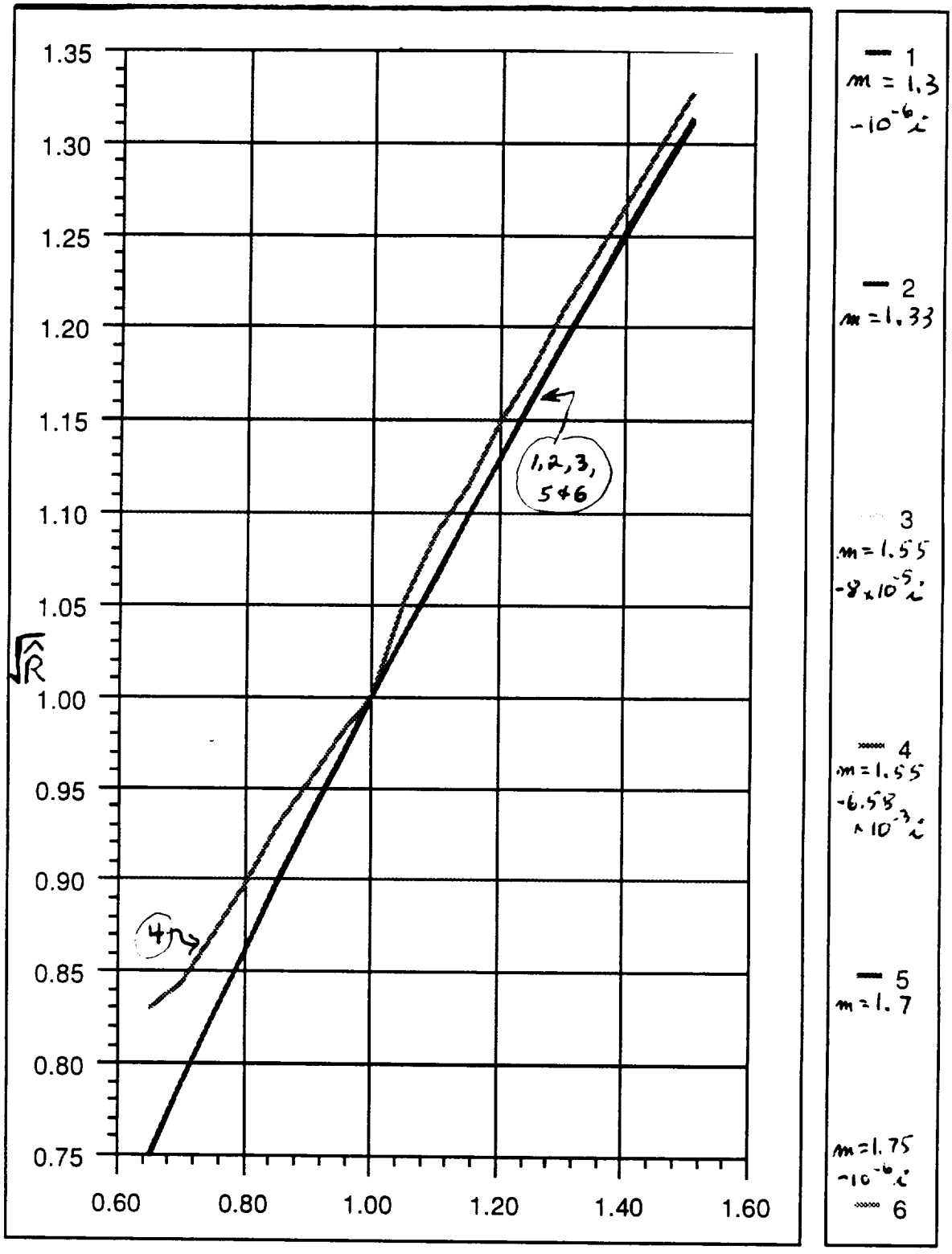

FIGURE 5: Average Ratio ($\sqrt{\hat{R}}$) Versus Eccentricity (ϵ)

It is also seen that the dependence of average ratio of amplitudes $\sqrt{(\hat{R})}$ on eccentricity is almost linear, over the range of refractive indices chosen for this graph.

6. Discussion

The high-frequency dependence of amplitude ratio on the radius makes fine inferences regarding radius difficult. However, the fact that the amplitude ratio varies in a somewhat narrow band, around a definite mean, which is constant over a range of radii, offers the prospect of performing gross analysis which is meaningful. Also encouraging is the striking empirical result that this mean value is independent of refractive index for a large range of indices.

The above mentioned material is intended to provide a more comprehensive insight into the factors affecting the error phenomena under investigation here. Thus the graphs permit the reader to infer trends, and otherwise apply the results to a variety of specific parameters that may pertain.

The above data has been translated into a format that lends itself more readily to the interpretation of actual sizing uncertainties. In Figures 6, 7, and 8, three separate graphs are plotted, for three different indices of refractions m; we present $m = 1.33$ in Figure 6, $m = 1.55$ in Figure 7, and $m = 1.75$ in Figure 8. The abscissas are the particle radii, and the ordinates are proportional to the scattering intensities. Each of these depicts two curves, the left (upper) one representing an eccentricity of 1.1 (the prolate spheroid case), the right (lower) one representing an eccentricity of 0.9 (the oblate spheroid case). The *horizontal separation* between the two curves at any given ordinate level is a direct measure of the sizing error at the associated sphere diameter (which is located roughly halfway between the two curves).

Visual inspection of these curves, which suggests that the sizing error might be directly proportional to the spheroid diameter, is in conformity with the conclusions drawn from the amplitude data above. This has been borne out by numerical analysis of the graphical data, which reveals a constant of proportionality of about $\pm 3.8\%$ for eccentricity of 1 ± 0.1. This constant has also been found to be directly proportional to the *eccentricity*, (e.g., $\pm 7.6\%$ for eccentricity 1 ± 0.2).

Note that the indices of refraction are all real; the results for complex indices develop rather severe oscillations beyond 15 micron radius. This phenomenon is believed to be an artifact of the approximation formula and remains to be explored further.

7. Summary

The spheroid approximation to non-spherical particles has yielded the extremely simple result that the sizing error is proportional to:

(1) the eccentricity, and
(2) the particle size.

It should be added, however, that the specific numerical value derived from the analysis, is subject to some uncertainty, owing to two separate simplifying assumptions, namely:

(1) that the forward scattering angle is 0 (instead of $1.6 - 2.6$ degrees), and
(2) that the alignment angle of the spheroid is also 0 (whereas a priori this is arbitrary).

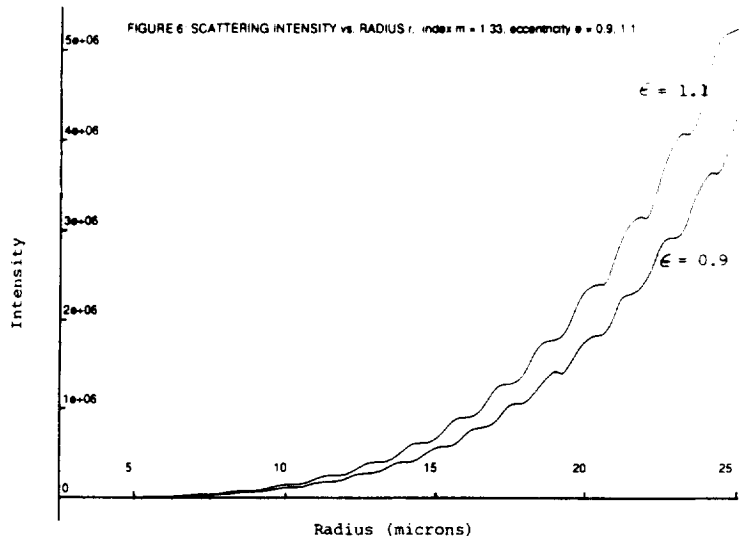
FIGURE 6: SCATTERING INTENSITY vs. RADIUS r, index m = 1.33, eccentricity e = 0.9, 1.1
Intensity
5e+06
4e+06
3e+06
2e+06
1e+06
0
5
10
15
20
25
Radius (microns)
ϵ = 1.1
ϵ = 0.9

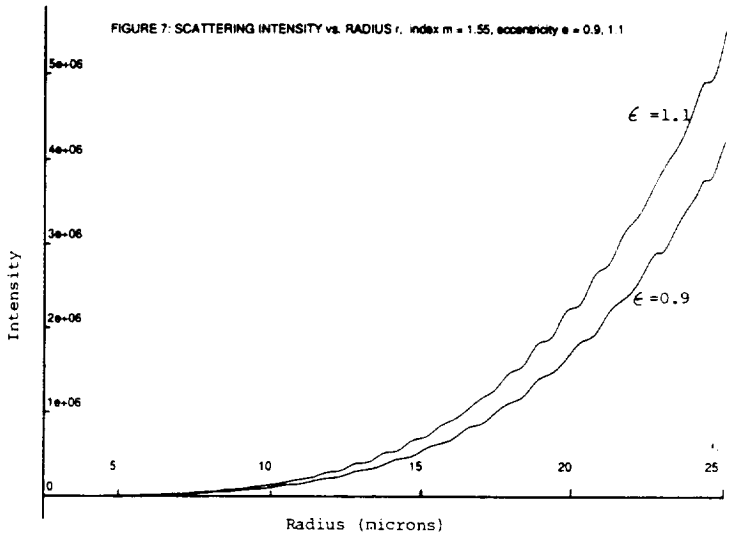
FIGURE 7: SCATTERING INTENSITY vs. RADIUS r, index m = 1.55, eccentricity e = 0.9, 1.1
Intensity
5e+06
4e+06
3e+06
2e+06
1e+06
0
5
10
15
20
25
Radius (microns)
ϵ =1.1
ϵ =0.9

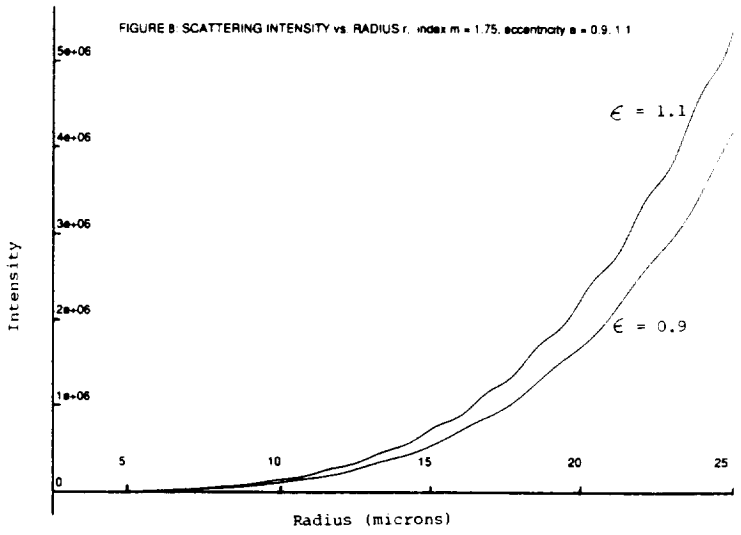
FIGURE 8: SCATTERING INTENSITY vs. RADIUS r, index m = 1.75, eccentricity e = 0.9, 1.1
Intensity
5e+06
4e+06
3e+06
2e+06
1e+06
0
5
10
15
20
25
Radius (microns)
ϵ = 1.1
ϵ = 0.9

While one can argue intuitively on physical grounds that the use of non-zero values should not materially alter these conclusions, it nevertheless remains to be corroborated by somewhat more rigourous mathematical investigation.

REFERENCES

1. A.R. Holt and J.W Shepherd: "Electromagnetic Scattering by dielectric spheroids in the forward and backward directions". J. Phys. A: Math. Gen., Vol. 12, No. 1, 1979. 159-166.
2. R.G. Newton: "Scattering theory of waves and particles", McGraw Hill, New York (1966)
3. H.C. Van de Hulst: "Light Scattering by Small Particles",Wiley, New York (1957).

8. The C source code "eccen.c" and the subroutine "scatamp"

```
/* start of scatamp.c subroutine file */
/* scatamp.c */

#include <math.h>

typedef struct{
   double x,y;
} cmplx;

extern cmplx cxadd();
extern cmplx cxsubtract();
extern cmplx cxmultiply();
extern cmplx cxconjugate();
extern double cxabs();
extern cmplx cxdivide();
extern cmplx cxexp();
extern cmplx cxsin();
extern cmplx cxcos();
extern void prntcx();
extern cmplx rcmultiply();
extern cmplx rcpromote();

cmplx scatamp(a,c,m,lambda,theta)
/*
   Calculates the forward scattering amplitude *f0
   for a spheroid with major axis a and minor axic c
   given the index of refraction m,
   the wavelength lambda,
   and the angle theta.
   FROM:
     Electromagnetic scattering by dielectric spheroids
     in the forward and backward directions.
     A.R. Holt and J.W. Shepherd
     J. Phys. A: Math. Gen., vol. 12, no. 1 (1979)
*/
double a;
double c;
cmplx m;
double lambda;
double theta;
{
   double k,denom,sqdenom,ss,cc,temp;
   cmplx mu,i,cxtemp;
   cmplx term1,term2,term3,term4,term5,term6,term7,term8,term9;
```

```
   k = 2.0*M_PI/lambda;
   i.x=0.0;i.y=1.0;
   ss=sin(theta);cc=cos(theta);
   denom = (ss*ss)/(a*a) + (cc*cc)/(c*c);
   sqdenom = sqrt(denom);
   temp = 2.0*k/sqdenom;
   cxtemp.x = m.x-1.0;cxtemp.y=m.y;
   mu = rcmultiply(temp,cxtemp);
   term1 = cxmultiply(mu,mu);
   term2.x = 0.0;term2.y = k*a*a*c*sqdenom;
   term3 = cxdivide(term2,term1);
   term4 = rcmultiply(0.5,term1);term4.x += 1.0;
   term5 = cxcos(mu);
   term6 = cxmultiply(mu,cxsin(mu));
   term7 = cxmultiply(i,cxsin(mu));
   term8 = cxmultiply(i,cxmultiply(mu,cxcos(mu)));
   term9 = cxsubtract(term4,term5);
   term9 = cxsubtract(term9,term6);
   term9 = cxsubtract(term9,term7);
   term9 = cxadd(term9,term8);
   term9 = cxmultiply(term3,term9);
   return(term9);
}
/* end of scatamp.c subroutine file */

/* start of eccen.c main file */
/* eccen.c */

#include <stdio.h>
#include <math.h>

typedef struct{
   double x,y;
} cmplx;

extern double cxabs();
extern cmplx scatamp();

void majminaxes();

void main()
{
   double lambda;  /* wavelength */
   cmplx  m;       /* index of refraction */
   double theta;   /* angle */
   double r;       /* radius of sphere */
```

```
   double e;       /* eccentricity */
   double a;       /* major axis of spheroid */
   double c;       /* minor axis of spheroid */
   double rat;     /* ratio of amplitudes */
   double af0,afs0;
   FILE *fpout,*fpin;
   double elo,ehi,estep,rlo,rhi,rstep,ratlo,rathi,ratstep;
   double e0,e1,emid,tol,rat0,rat1,ratmid,error,sign;
   char outname[80];
   double rattable[50],ratavg[50];
   int i,n,k;

/*  read input file mie4_input.dat */
fpin=fopen("mie4_input.dat","r");
fscanf(fpin,"theta %lf\n",&theta);
fscanf(fpin,"lambda %lf\n",&lambda);
fscanf(fpin,"mx %lf\n",&(m.x));
fscanf(fpin,"my %lf\n",&(m.y));
fscanf(fpin,"elo %lf\n",&elo);
fscanf(fpin,"ehi %lf\n",&ehi);
fscanf(fpin,"estep %lf\n",&estep);
fscanf(fpin,"rlo %lf\n",&rlo);
fscanf(fpin,"rhi %lf\n",&rhi);
fscanf(fpin,"rstep %lf\n",&rstep);
fscanf(fpin,"output %s\n",outname);
fclose(fpin);


   fpout = fopen(outname,"w");
   fprintf(fpout,"theta = %lf\n",theta);
   fprintf(fpout,"lambda = %lf\n",lambda);
   fprintf(fpout,"m = %lf + %lfI\n\n",m.x,m.y);

   n=1+(int)((ehi-elo)/estep);

   for(i=0;i<n;i++) fprintf(fpout,"radius\t%8.3lf\t",elo+i*estep);
   fprintf(fpout,"\n");

   for(i=0;i<n;i++) ratavg[i]=0.0;
   k=0;
   for(r = rlo;r <= rhi;r += rstep){
      printf("radius = %lf\n",r);
      afs0=cxabs(scatamp(r,r,m,lambda,theta));
      for(i=0;i<n;i++){
         e=elo+i*estep;
         majminaxes(r,e,&c,&a);
```

```
            rat=cxabs(scatamp(a,c,m,lambda,theta))/afs0;
            rattable[i]=rat;
            ratavg[i] += rat;
         } /* end of i for */
         for(i=0;i<n;i++) fprintf(fpout,"%lf\t%lf\t",r,rattable[i]);
         fprintf(fpout,"\n");
         k++;
      } /* end of r for */
      for(i=0;i<n;i++){
         ratavg[i] /= k;
         fprintf(fpout,"%lf\t%lf\n",elo+i*estep,ratavg[i]);
      }
      fclose(fpout);
}

void majminaxes(r,e,c_ptr,a_ptr)
/* given radius r of a shere, and desired eccentricity e,
   returns the major axis a and minor axis c
   of a spheroid with the same volume
   and that eccentricity.
*/
double r;
double e;
double *c_ptr;
double *a_ptr;
{
   *c_ptr = r*pow(e,-0.66666666666);
   *a_ptr = (*c_ptr)*e;
}
/* end of eccen.c main file */
```

FT. COLLINS, CO 80525

BEDFORD, MA 01730

NASA
National Aeronautics and Space Administration

Report Documentation Page

1. Report No.	2. Government Accession No.	3. Recipient's Catalog No.

4. Title and Subtitle

FINAL REPORT

TITLE: Spacecraft Particulate Sizing Spectrometer

5. Report Date

7 April, 1992

6. Performing Organization Code

7. Author(s)

Henry A. Miranda, Jr.

8. Performing Organization Report No.

10. Work Unit No.

9. Performing Organization Name and Address

MIRANDA LABORATORIES
74 Loomis Street, Bedford, MA 01730

11. Contract or Grant No.

NAS5-30306

12. Sponsoring Agency Name and Address

NASA, Washington, DC 20546-0001

13. Type of Report and Period Covered

FINAL -
15 Sept/89 to present

14. Sponsoring Agency Code

15. Supplementary Notes

16. Abstract

An evaluation prototype device recently delivered to NASA/GSFC as an end-item under the subject Contract, is described, together with conclusions and several recommendations for follow-on flight hardware. The device detects individual particles crossing an external sensing zone, and produces a histogram displaying the size distribution of particles sensed, over the nominal range 5-50 microns.

The output is totally independent of particle refractive index, and is also largely unaffected by particle shape, (the reported diameters being in terms of the equivalent sphere, as judged by the scattered light intercepted by the receiving channels, which develop signals whenever a particle crosses the beam of illumination in the sensing zone.

Supporting evidence for the latter assertion is discussed in the body of the report, based upon experimental test data for non-spherical particulates. Also included is a technical appendix which presents theoretical arguments that provide a firm foundation for this assertion.

17. Key Words (Suggested by Author(s))	18. Distribution Statement
Particle sizing Spacecraft environment Remote particle sensing Forward scattering	Unclassified - unlimited

19. Security Classif. (of this report)	20. Security Classif. (of this page)	21. No. of pages	22. Price
Unclassified	Unclassified	26	A0a (/)

NASA FORM 1626 OCT 86